

Evidence for two energy scales in the superconducting state of optimally doped $(\text{Bi,Pb})_2(\text{Sr,L a})_2\text{CuO}_{6+\delta}$

Takeshi Kondo,^{1,2} Tsunehiro Takeuchi,^{1,3} Adam Kaminski,² Syunsuke Tsuda,⁴ and Shik Shin⁴

¹*Department of Crystalline Materials Science, Nagoya University, Nagoya 464-8603, Japan*

²*Ames Laboratory and Department of Physics and Astronomy, Iowa State University, Ames, IA 50011, USA*

³*EcoTopia Science Institute, Nagoya University, Nagoya 464-8603, Japan*

⁴*Institute of Solid State Physics, University of Tokyo, Kashiwa 277-8581, Japan*

(Dated: May 15, 2019)

We use angle-resolved photoemission spectroscopy (ARPES) to investigate the properties of the energy gap(s) in optimally doped $(\text{Bi,Pb})_2(\text{Sr,L a})_2\text{CuO}_{6+\delta}$ (Bi2201). We find that the spectral gap has two components in the superconducting state: a superconducting gap and pseudogap. Significant differences in their momentum and temperature dependence suggest that they represent two separate energy scales. Spectra near the node reveal a sharp peak with a small gap below T_c that closes at T_c . Near the antinode, the spectra are broad with a large energy gap of $\sim 40\text{meV}$ above and below T_c . The spectral shape and gap magnitude around the antinode are almost constant across T_c , which indicates that the pseudogap state coexists with the superconducting state below T_c , and it dominates the character of the spectra around the antinode. We speculate that the pseudogap state competes with the superconductivity by diminishing spectral weight in the antinodal regions, where the magnitude of the superconducting gap is largest.

PACS numbers:

The pseudogap is one of the most fascinating properties of the high temperature superconductors¹. It gives rise to a strange state of matter above T_c where parts of the Fermi surface consist of disconnected "arcs"², while the remainder is gapped. Recent Angle Resolved Photoemission Spectroscopy (ARPES) measurements show that the pseudogap state extrapolates at absolute zero to a nodal liquid where the Fermi surface consists of just four points³. Since the pseudogap is often closely linked to the mechanism of high temperature superconductivity, it is very important to understand its properties and relationship to the superconducting gap. According to one class of theories⁴, the pseudogap opens because electrons are paired at temperatures much higher than the critical temperature (T_c) with the same pairing mechanism as the superconducting gap. The pairs only condense when the sample is cooled to T_c . This scenario is supported by a number of ARPES studies on mostly $\text{Bi}_2\text{Sr}_2\text{Ca}_2\text{O}_{8+\delta}$ (Bi2212) suggesting that the behavior and symmetry of the pseudogap above T_c are similar to those of the superconducting gap below T_c ^{5,6,7}. Another class of theories^{8,9,10} link the pseudogap to an ordered state with possibly a separate energy scale. The first ARPES experiment designed to detect an ordered state below the pseudogap temperature gave a positive result¹¹. However, a later ARPES experiment was unable to detect the same small signatures in the data¹². More recently, a high precision neutron scattering experiment provided direct evidence for the existence of an ordered state of particular symmetry below the pseudogap temperature¹³. This result confirmed the predictions of Varma and was in agreement with the first ARPES study. Recent scanning tunneling microscopy and scanning tunneling spectroscopy (STM/STS) experiments on Bi2212 show that even below T_c , a pseudogap state, char-

acterized by a large gap and broad spectral peaks, coexists with the superconducting state, which has a smaller energy gap and sharp spectral peaks^{14,15}. One drawback of studying the pseudogap in Bi2212 is its very large superconducting gap ($\sim 40\text{ meV}$ at optimal doping), which is comparable to the pseudogap. We chose to study $(\text{Bi,Pb})_2(\text{Sr,L a})_2\text{CuO}_{6+\delta}$ (Bi2201), which has a low T_c of $\sim 35\text{K}$ at optimal doping. NMR¹⁶ and electrical resistivity¹⁷ experiments estimate the pseudogap temperature in Bi2201 to be similar to that of Bi2212, while T_c is almost three times smaller. Therefore, we should gain an important insight into the relationship between the pseudogap and the superconducting gap by directly measuring the energy gap in Bi2201. In this letter, we report ARPES measurements of the momentum- and temperature-dependence of the energy gap in optimally doped Bi2201 with $T_c = 35\text{K}$. On first inspection, the momentum dependence of the energy gap below T_c strongly deviates from the symmetry of a monotonic $d_{x^2-y^2}$ wave function, which is observed in optimally doped Bi2212¹⁸. The gap symmetry and its temperature dependence are most consistent with a two gap component model: a small $d_{x^2-y^2}$ wave superconducting gap that dominates the symmetry near the node and a large pseudogap that exists only around the antinode.

We measured optimally doped single crystals of $(\text{Bi,Pb})_2(\text{Sr,L a})_2\text{CuO}_{6+\delta}$ ($T_c = 35\text{K}$) that were grown using a conventional floating-zone (FZ) technique and subsequent annealing¹⁹. T_c was determined from susceptibility and electrical resistivity measurements and the samples had a sharp superconducting transition ($\sim 3\text{meV}$). Pb was used to substitute for Bi in order to suppress the modulation of the BiO plane. This normally leads to a contamination of the ARPES signal from umklapp replicas of the main band. The use of modulation-free samples

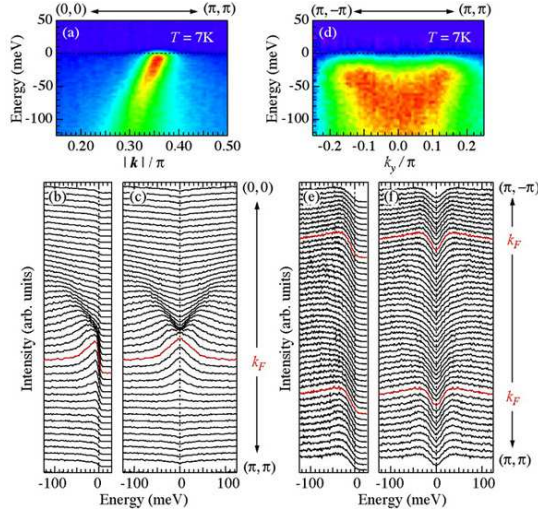


FIG. 1: (color online) ARPES intensity and the corresponding EDCs measured at 7K well below T_c along (a,b) $(0,0)$ - (π,π) and (d,e) $(\pi,-\pi)$ - (π,π) cut. (c,f) Symmetrized EDC of (b,c).

enabled us to precisely determine the energy gap. The measurements were made using a Scienta SES2002 hemispherical analyzer with a Gammadata VUV5010 photon source (HeI α) at the Institute of Solid State Physics (ISSP), the University of Tokyo. The energy and angular resolutions were 5meV and 0.13° , respectively.

In Fig. 1 (a,b) and (d,e), we show the ARPES data (intensity plots and the corresponding Energy Distribution Curves, EDCs) measured at 7K well below T_c in the nodal and antinodal regions, respectively. The nodal spectra are characterized by sharp peaks. The leading edge of the EDC at the nodal k_F reaches the Fermi level, indicating there is no energy gap. The spectra at the antinodal cut, in contrast, are very broad. EDCs near the antinodal k_F are shifted towards higher binding energies due to the presence of an energy gap. This effect is illustrated more easily in Fig. 1 (c) and (f) by use of a symmetrization method². EDCs are reflected about the Fermi level and added to the original data. This technique removes the Fermi function and enables us to immediately identify the presence of an energy gap. Clearly, a gap is present in the data of Fig. 1 (f) and is absent in Fig. 1 (c).

Figure. 2(a) shows the ARPES intensity at the Fermi level. The intensity is strongest near the node and diminishes towards the antinode $(\pi,0)$. This is a clear signature of an anisotropic energy gap. We determined the size of the energy gap using two methods. The first estimates the shift in energy of the mid point of the EDC leading edge (Δ_{mid}). Figure 2(b) shows the EDCs measured at different k_F for angles ϕ , defined in the inset of Fig. 2(d). The leading edge shift is zero at the node ($\phi = 45^\circ$), and it increases toward the antinode ($\phi = 0^\circ$). The second method determines the peak position of the symmetrized EDC (Δ_{peak}). Figure 2(c) shows results from this method with the peak positions marked by arrows. Results from both methods are compared in Fig. 2(d). It is clear that

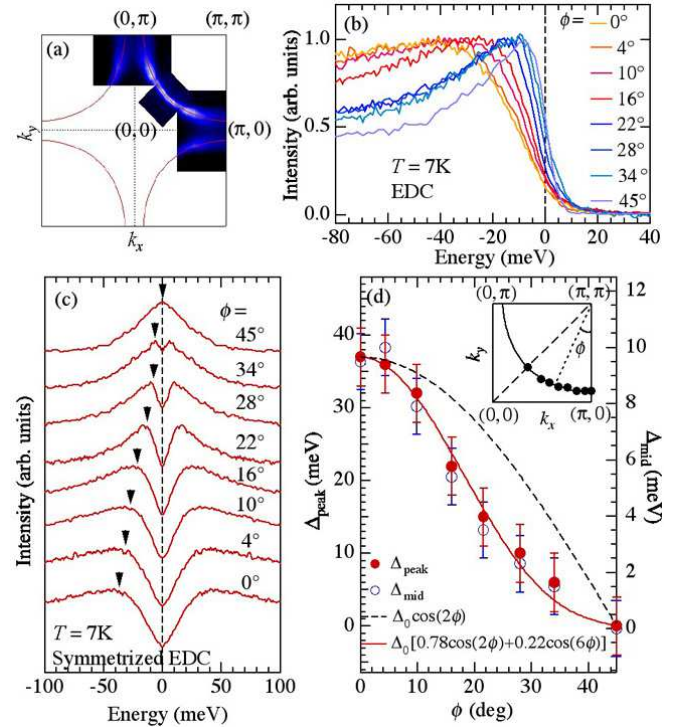


FIG. 2: (color online) (a) ARPES intensity map around the Fermi level as a function of k_x and k_y . (b) EDC and (c) symmetrized EDC measured at $T = 7\text{K}$ (well below T_c) for various k_F . The angle ϕ is defined in the inset of (d). (d) Magnitude of the energy gap around the Fermi surface at $T = 7\text{K}$ estimated from the mid-point of the EDC leading edge (Δ_{mid}) and the peak position in the symmetrized EDC (Δ_{peak} - indicated by the arrows in (c)). The solid line shows a gap function of the form $\Delta(\phi) = \Delta_0[0.78 \cos(2\phi) + 0.22 \cos(6\phi)]$ (dashed line corresponds to $\Delta(\phi) = \Delta_0 \cos(2\phi)$).

both methods show the gap increases towards the antinode. Although the maximum values are different for obvious reasons, both yield a similar symmetry of the gap. A remarkable feature in the energy gap is the strong deviation from a monotonic $d_{x^2-y^2}$ -wave symmetry, which is illustrated by the dashed line in Fig. 2(d). Harris *et al.*²⁰ first reported this feature in Bi2201 about a decade ago, and suggested that the enhanced anisotropy is caused by impurity scattering which results in a strong suppression of the energy gap close to the node. The authors measured samples with a large residual resistivity ratio, $\rho_{ab}(300\text{K})/\rho_{ab}(0\text{K})$, of 2.4, so idea of an impurity-induced gap symmetry seemed plausible²¹. (Here, ρ_{ab} represents the resistivity along the CuO_2 plane, and $\rho_{ab}(0\text{K})$ was estimated from an interpolation to $T = 0\text{K}$.) In this work, we employed high quality single crystals with a low $\rho_{ab}(300\text{K})/\rho_{ab}(0\text{K})$ ratio of ~ 7 , yet we observe a similar deviation from the monotonic $d_{x^2-y^2}$ -wave symmetry. Hence, impurities are unlikely to be the cause of the characteristic gap symmetry in Bi2201.

It has been reported that the superconducting gap also significantly deviates from a monotonic $d_{x^2-y^2}$ -wave sym-

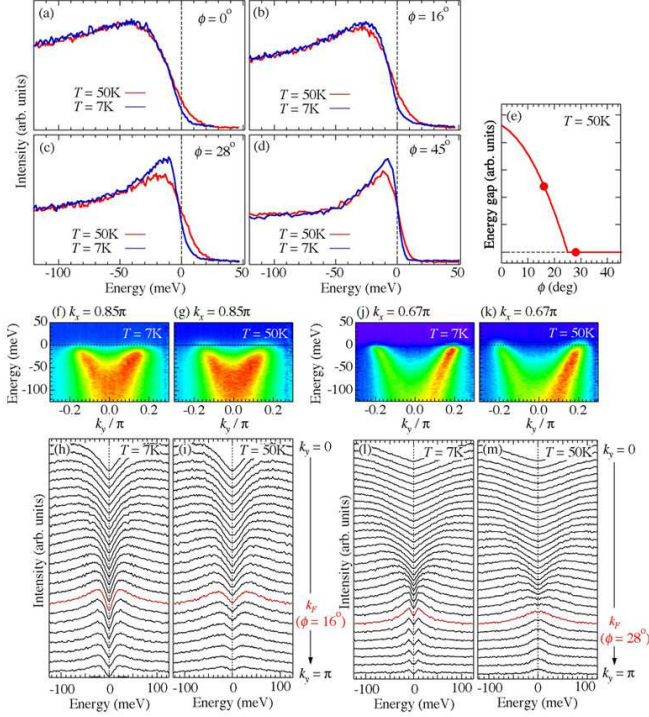


FIG. 3: (color online) (a,b,c,d) EDC below and above T_c (7K and 50K) at various k_F 's ($\phi = 0^\circ, 16^\circ, 28^\circ$, and 45°). (e) Schematic illustration of the energy gap above T_c as a function of the angle ϕ . The two solid circles correspond to the energy gap at $\phi = 16^\circ$ and 28° . ARPES intensity map and the corresponding symmetrized EDCs measured along a momentum cut at $k_x = 0.85\pi$ crossing k_F of $\phi = 16^\circ$ (f,g,h,i) and at $k_x = 0.65\pi$ crossing k_F of $\phi = 28^\circ$ (j,k,l,m). (The contrast of the ARPES intensity between the positive and negative k_y is caused by the matrix element effect.) Left and right hand panels were obtained at $T = 7\text{K}$ and 50K , respectively.

metry in underdoped Bi2212²². This was attributed to an increase of the electron correlation with underdoping, which may increase the intensity of the higher order harmonic component in the d -wave gap function. We fitted a function of the form $\Delta(\phi) = \Delta_0[B \cos(2\phi) + (1 - B) \cos(6\phi)]$ to the energy gap in the present data, with a $\cos(6\phi)$ second order harmonics term in the $d_{x^2-y^2}$ -wave. The result is plotted in Fig. 2(d) using a solid line. Even though our Bi2201 samples are optimally doped we find a much stronger deviation from a pure $d_{x^2-y^2}$ symmetry ($B = 0.78$) compared to underdoped Bi2212 with $T_c = 75\text{K}$ ($B = 0.88$)²². Hence, the deviation in Bi2201 is unlikely to be due to strong correlation effects.

Figure 3 (a)-(d) show EDCs at four k_F s above and below T_c (7K and 50K). Spectra near the node (Fig.3 (c) and (d)) vary significantly across T_c ; the sharp peak below T_c broadens above T_c and the energy gap closes slightly away from the node. This is contrasted by very little variation in the spectral line shape near the antinode across T_c (Fig.3 (a) and (b)). The main feature here is a slight increase in spectral intensity above T_c

very close to the Fermi level. The two extreme behaviors evolve rapidly with momentum as evident by comparing panels (f-i) and (j-m). They show the ARPES intensity and symmetrized EDCs measured along two momentum cuts crossing k_F at angles $\phi = 16^\circ$ and 28° , respectively. Above T_c , the gap closes at k_F corresponding to $\phi = 28^\circ$. For $\phi = 16^\circ$ the symmetrized EDC shows a weak variation in the spectral line shape and has an almost unchanged peak position. This generates a large Fermi arc above T_c schematically illustrated in Fig. 3 (e). Previous results from Bi2212^{2,5} reported a small spectral variation with increasing temperature in the pseudogap state above T_c . Therefore our current data on Bi2201 indicates that the energy gap near the antinode is dominated by the pseudogap even below T_c .

In order to investigate the pseudogap state, we measured ARPES spectra over a wide temperature range. The resulting symmetrized EDCs are superimposed in Fig. 4(a)-(d) for several k_F s. The pseudogap is quite large up to 100K and closes at $\sim 150\text{K}$. In optimally doped Bi2212, the pseudogap closing temperature (T_{PG}) has been estimated to be $\sim 130\text{K}$ by ARPES²³. Thus the present results indicate that the pseudogap (characterized by the energy gap size and T_{PG}) does not scale with T_c in optimally doped high- T_c cuprates. In Fig. 4 (i), we plot the measured energy gap (Δ_{peak}) as a function of angle ϕ at several temperatures ranging from below T_c to above T_{PG} . We also plot the monotonic $d_{x^2-y^2}$ -wave function for the superconducting gap of optimally doped Bi2212^{18,22} (solid black line) and that scaled by the ratio of the T_c s in optimally doped Bi2201 and Bi2212 (dashed line). Around the node, the gap symmetry at 7K is consistent with the $d_{x^2-y^2}$ -wave gap function (dashed line). This component disappears above T_c . The energy gap rapidly increases towards the antinode and its maximum value is very similar to that in optimally doped Bi2212. The characteristic gap symmetry below T_c in optimally doped Bi2201, therefore, can be understood as a coexistence of the superconducting state with a small gap ($\sim 15\text{meV}$) that has a monotonic $d_{x^2-y^2}$ -wave symmetry and a pseudogap state that has a large energy gap similar to that of optimally doped Bi2212. The former dominates the spectral lineshape around the node, while the latter dominates at the antinodal region. In Bi2212, the superconducting gap has a similar energy size as the pseudogap ($\sim 40\text{meV}$ at the antinode), thus these two different gaps are continuously connected across T_c and appear to have the same origin^{5,6}. In Bi2201 the superconducting gap is much smaller, due to its low T_c , whereas the pseudogap remains large. The very different properties of these two gaps around the Fermi surface lead us to conclude there is no direct relationship between the pseudogap and superconducting gap.

Finally, we should comment that while the spectral peak position is a good way to investigate the momentum behavior of the energy gap in the pseudogap state (Fig. 4 (i)), this is not true for its temperature dependence. We found that, similar to Bi2212^{2,24}, the peak position

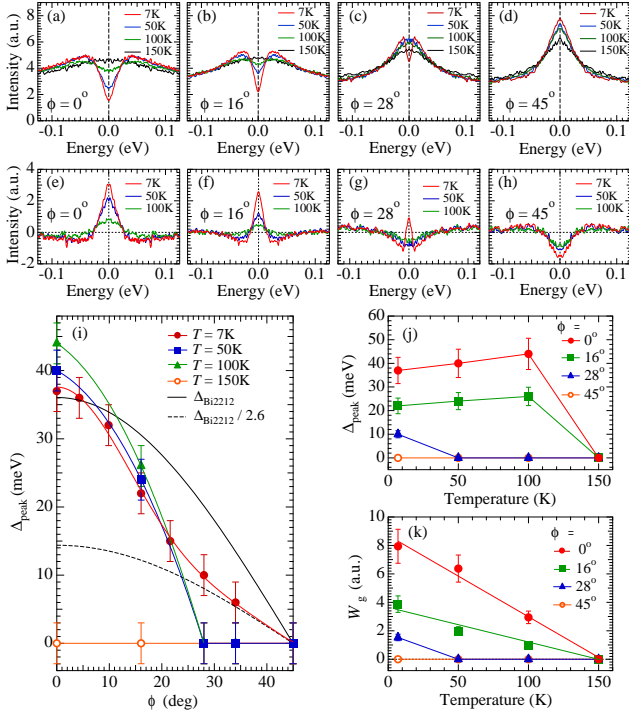


FIG. 4: (color online) (a,b,c,d) Symmetrized EDCs at various k_F ($\phi = 0^\circ, 16^\circ, 28^\circ$, and 45°) and temperatures. (e,f,g,h) The symmetrized EDC at $T = 150\text{K}$ (above the pseudogap closing temperature, T_{PG}) subtracted by one at 7K, 50K, and 100K. (i) ϕ dependence of Δ_{peak} from below T_c to above T_{PG} . The solid black line shows Δ_{peak} for optimally doped Bi2212 ($\Delta_{\text{Bi2212}} \propto \cos(2\phi)$). The dashed black line shows Δ_{Bi2212} divided by 2.6 ($\approx T_c(\text{Bi2212})/T_c(\text{Bi2201}) = 90\text{K}/35\text{K}$). (j) Peak position of the symmetrized EDC (Δ_{peak}) as a function of temperature. (k) Spectral weight lost due to the gap-opening near the Fermi energy (W_G) as a function of the temperature.

of the symmetrized EDCs around the antinode increases with increasing temperature below the pseudogap closing temperature (T_{PG}) and suddenly jump to zero above T_{PG} as illustrated in Fig. 4(j). This behavior should be contrasted with the continuous temperature dependence

of the symmetrized spectral shape below T_{PG} (Fig. 4 (a-d)). The significant temperature dependence of the pseudogap is illustrated by subtracting the symmetrized EDC below T_{PG} from that above T_{PG} as shown in Fig. 4(e-h). Here we note that when the energy gap is zero as shown at the node (Fig. 4(d)), the difference spectrum has a dip (Fig. 4(h)) because it simply reflects the thermal broadening of the spectral peak. The difference spectrum has a peak when the energy gap is finite, reflecting the loss of spectral weight due to the energy gap. We estimated the spectral weight lost when the gap opens (W_G) from the area of the spectral peak in Fig. 4(e-h), and plot it in Fig. 4 (k). Near the node, W_{PG} is zero above T_c because the superconducting gap closes. In contrast, W_G around the antinode decreases with increasing temperature in an almost linear fashion up to T_{PG} . The behavior of W_{PG} without a jump across T_c supports the idea that the ARPES spectrum around the antinode is dominated by the pseudogap state even below T_c .

In conclusion we report the momentum and temperature dependence of the energy gap measured by ARPES in an optimally doped single layer cuprate Bi2201 with $T_c = 35\text{K}$. While the superconducting gap, which closes at T_c , is observed around the node, the ARPES spectra is dominated by the pseudogap state below T_c around the antinode, where the spectral weight close to the Fermi level fills in with increasing temperature with a T -linear behavior. Significant differences in the momentum and temperature dependence of the pseudogap and superconducting gap force us to conclude there is no direct relationship between the two gaps. This points to the possibility of a competition between the pseudogap and superconducting gap.

We thank M. R. Norman, H. M. Fretwell and C. M. Varma for useful remarks. This work was supported by Director Office for Basic Energy Sciences, US DOE. The Ames Laboratory is operated for the US DOE by Iowa State University under Contract No. W-7405-ENG-82.

Note added: After completion of this work, we became aware of related work by K. Tanaka *et al.*, Science Express: 10.1126/science.1133411 that reached similar conclusions using data from underdoped Bi2212 samples.

- ¹ T. Timusk and B. Statt, Rep. Prog. Phys. **62**, 61 (1999).
- ² M. R. Norman *et al.*, Nature **392**, 157 (1998).
- ³ A. Kanigel *et al.*, Nature physics **2**, 447 (2006).
- ⁴ V. J. Emery *et al.*, Nature **374**, 434 (1995).
- ⁵ H. Ding *et al.*, Nature **382**, 51 (1996).
- ⁶ A. G. Loeser *et al.*, Science **273**, 325 (1996).
- ⁷ J. C. Campuzano *et al.*, Phys. Rev. Lett. **83**, 3709 (1999).
- ⁸ T. C. Hsu, J. B. Marston, and I. Affleck, Phys. Rev. B. **43**, 2866 (1991).
- ⁹ C. M. Varma, Phys. Rev. B. **55**, 14554 (1997).
- ¹⁰ C. M. Varma, Phys. Rev. Lett. **83**, 3538 (1999).
- ¹¹ A. Kaminski *et al.*, Nature **416**, 610 (2002).
- ¹² S. V. Borisenko *et al.*, Phys. Rev. Lett. **92**, 207001 (2004).

- ¹³ B. Fauqué *et al.*, Phys. Rev. Lett. **96**, 197001 (2006).
- ¹⁴ S. H. Pan *et al.*, Nature **413**, 282 (2001).
- ¹⁵ K. McElroy *et al.*, Phys. Rev. Lett. **94**, 197005 (2005).
- ¹⁶ Guo-qing Zheng *et al.*, Phys. Rev. Lett. **94**, 047006 (2005).
- ¹⁷ Yoichi Ando *et al.*, Phys. Rev. Lett. **93**, 267001 (2004).
- ¹⁸ H. Ding *et al.*, Phys. Rev. B **54**, R9678 (1996).
- ¹⁹ T. Kondo *et al.*, Phys. Rev. B **72**, 024533 (2005).
- ²⁰ J. M. Harris *et al.*, Phys. Rev. Lett. **79**, 143 (1997).
- ²¹ S. Haas *et al.*, Phys. Rev. B **56**, 5108 (1997).
- ²² J. Mesot *et al.*, Phys. Rev. Lett. **83**, 840 (1999).
- ²³ T. Sato *et al.*, Physica C **341-348**, 815 (2000).
- ²⁴ M. R. Norman *et al.*, Phys. Rev. B **57**, R11093 (1998).